A comparative study of α-$Ni(OH)_2$ and Ni nanoparticles supported ZIF-8@reduced graphene oxide- derived nitrogen doped carbon for electrocatalytic ethanol oxidation

Soliman Gamal, Doaa A Kospa, Amr Awad Ibrahim*, Awad I. Ahmed, A.M.A. Ouf

Department of Chemistry, Faculty of Science, Mansoura University, Al-Mansoura 35516, Egypt.

Supplementary data

Fig. S1: (a) N_2 adsorption-desorption isotherms and (b) the corresponding distributions of pore diameters of ZIF-8, ZIF@rGO, ZNC@rGO, and $Ni(OH)_2$/ZNC@rGO obtained from the desorption branch using the Barrett–Joyner–Halenda (BJH) method.

Fig. S2: XPS of GO, (a) Total survey and high-resolution spectra of (b) C1s and (c) O1s.

Fig. S3: (a) High magnification SEM image and (b) SEM of elemental mapping region of $Ni(OH)_2$/ZNC@rGO, and (c) EDX mapping of $Ni(OH)_2$/ZNC@rGO, (d) C, (e) O, (f) N, (g) Zn, and (h) Ni.

Fig. S4: EDX analysis of $Ni(OH)_2$/ZNC@rGO.

Fig. S5: CV curves of (a) ZIF-8, ZIF-8@rGO, and ZNC@rGO and (b) Ni/ZNC@rGO, α-$Ni(OH)_2$, and $Ni(OH)_2$/ZNC@rGO recorded at 50 mV s^{-1} in 1M KOH.

Fig. S6: CV curves recorded in 1M KOH in the potential range of 0- 0.1 V at different scan rates for (a) ZIF-8, (b) ZIF-8@rGO, (c) ZNC@rGO, (d) Ni/ ZNC@rGO, (e) α$Ni(OH)_2$, and (f) $Ni(OH)_2$/ ZNC@rGO.

Fig. S7: CV curves of (a) ZIF-8, (b) ZIF-8@rGO, (c) ZNC@rGO, (d) Ni/ ZNC@rGO, (e) α-$Ni(OH)_2$ and (f) $Ni(OH)_2$/ ZNC@rGO in the absence and presence of 1M ethanol at a scan rate of 50 mV s^{-1}.

Fig. S8: CV curve of the as-prepared catalysts in 1M KOH + 1M Ethanol at a scan rate of 50 mV s^{-1}.

Fig. S9: CV curves recorded in 1M KOH in the potential range of -0.2- 0.6 V at different scan rates for (a) ZIF-8@rGO, (b) ZNC@rGO, (c) Ni/ ZNC@rGO, (d) α-$Ni(OH)_2$, and (e) $Ni(OH)_2$/ ZNC@rGO catalysts.

Fig. S10: Linear relationship of anodic (I_{pa}) and cathodic current (I_{pc}) densities of (a) ZIF-8@rGO, (b) ZNC@rGO, (c) Ni/ZNC@rGO, and (d) α-$Ni(OH)_2$ versus the square root of scan rates.

Fig. S11: Linear relationship of anodic (I_{pa}) and cathodic current (I_{pc}) densities of (a) ZIF-8@rGO, (b) ZNC@rGO, (c) Ni/ZNC@rGO, and (d) α-$Ni(OH)_2$ versus the scan rates.

Fig. S12: CV of (a) ZIF-8@rGO, (b) ZNC@rGO, Ni/ ZNC@rGO, (d) α-$Ni(OH)_2$ and (e) $Ni(OH)_2$/ ZNC@rGO catalysts in 1M KOH with different concentrations of ethanol (0.1- 2.0 M).

Fig. S13: CV of $Ni(OH)_2$/ ZNC@rGO in (a) 1M of alkaline and acidic electrolyte and (b) 1M of EtOH+ 1M of alkaline or acidic medium.

Fig. S14: CV of (a) ZIF-8@rGO, (b) ZNC@rGO, (c) Ni/ ZNC@rGO, (d) α-$Ni(OH)_2$ and (e) $Ni(OH)_2$/ ZNC@rGO catalysts in 1M EtOH with different concentrations of KOH electrolyte (0.1- 2.0 M) and (f) effect of concentration of the KOH electrolyte in electrocatalytic ethanol oxidation.

Fig. S15: CVs curves for 900 cycles from -0.2- 0.6 V at a scan rate of 10 mV s^{-1} in 1M KOH+ 1M EtOH using Ni/ ZNC@rGO.

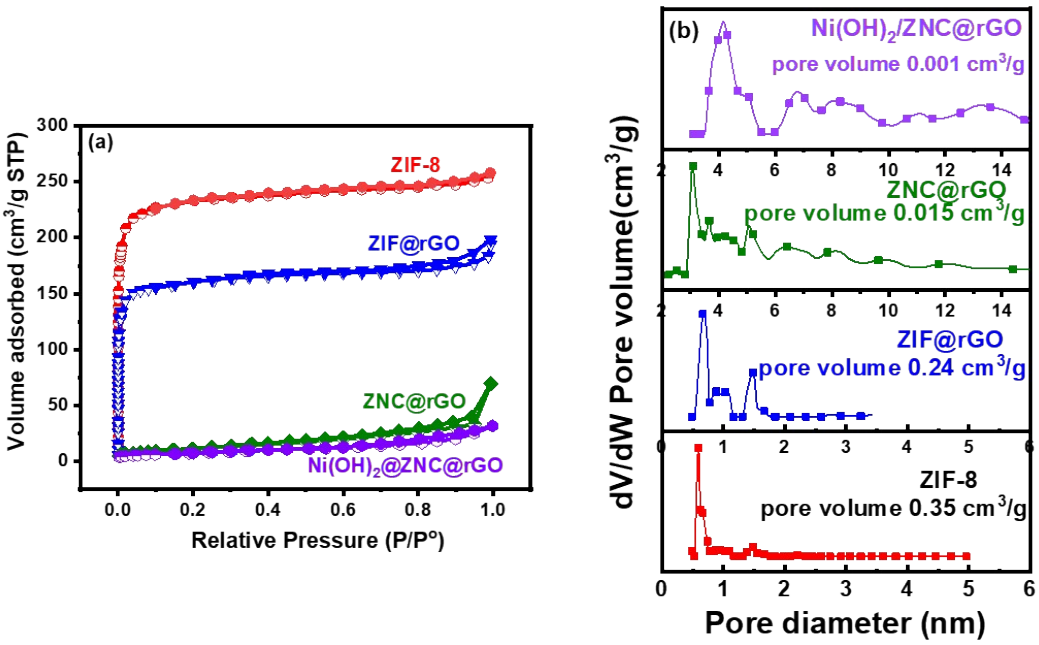

Fig. S1: (a) N_2 adsorption-desorption isotherms and (b) the corresponding distributions of pore diameters of ZIF-8, ZIF@rGO, ZNC@rGO, and $Ni(OH)_2$/ZNC@rGO obtained from the desorption branch using the Barrett–Joyner–Halenda (BJH) method.

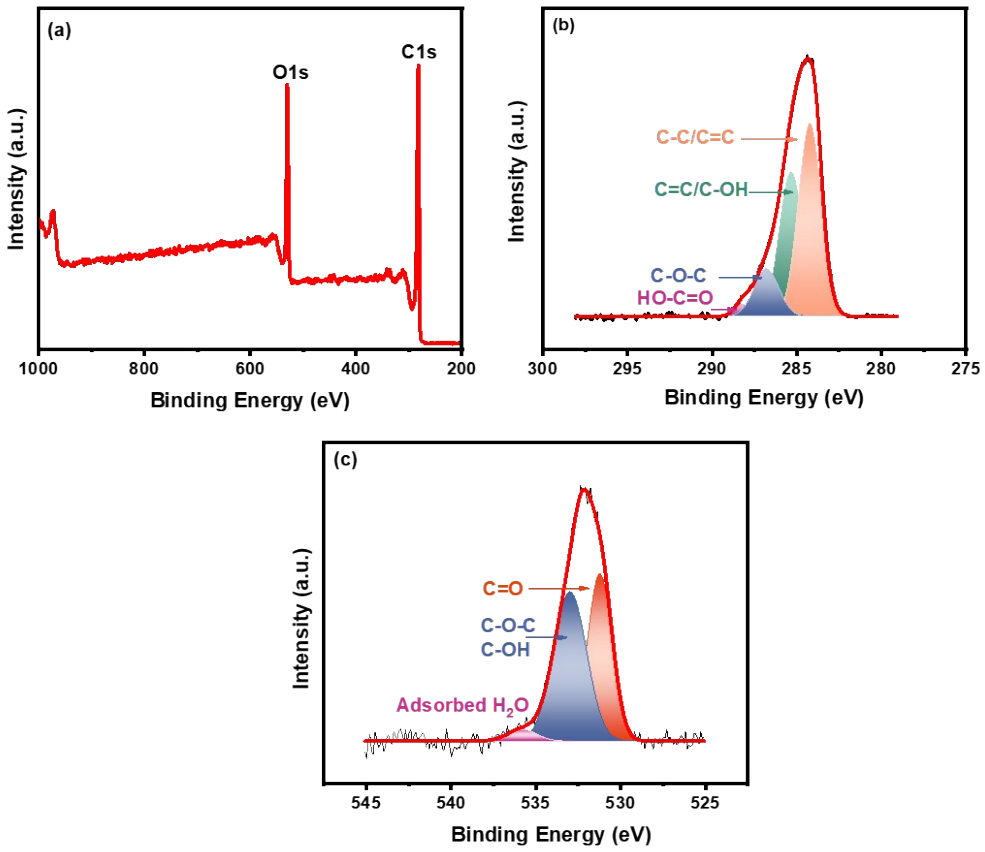

Fig. S2: XPS of GO, (a) Total survey and high-resolution spectra of (b) C1s and (c) O1s.

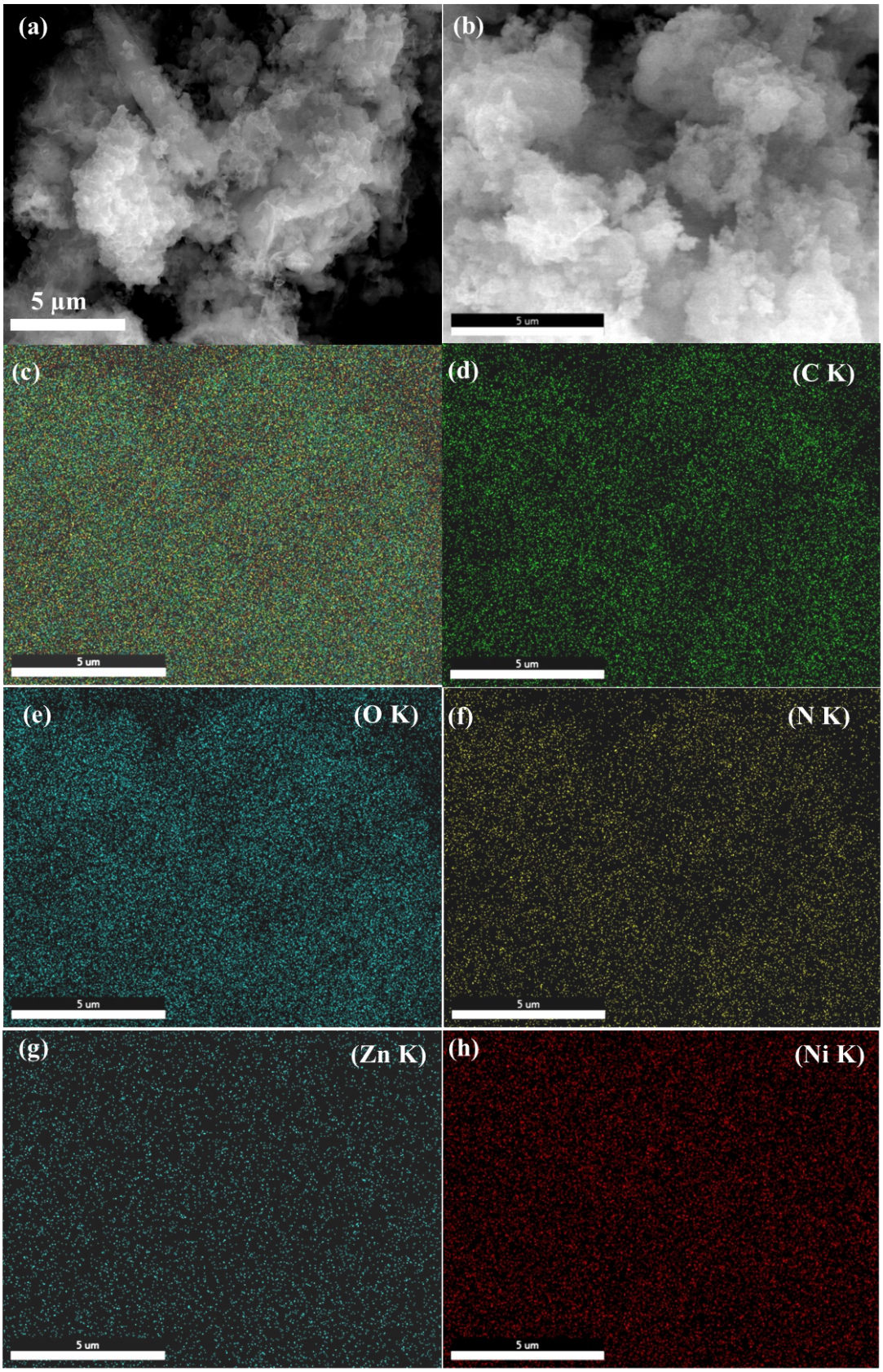

Fig. S3: (a) High magnification SEM image and (b) SEM of elemental mapping region of $Ni(OH)_2$/ZNC@rGO, and (c) EDX mapping of $Ni(OH)_2$/ZNC@rGO, (d) C, (e) O, (f) N, (g) Zn, and (h) Ni.

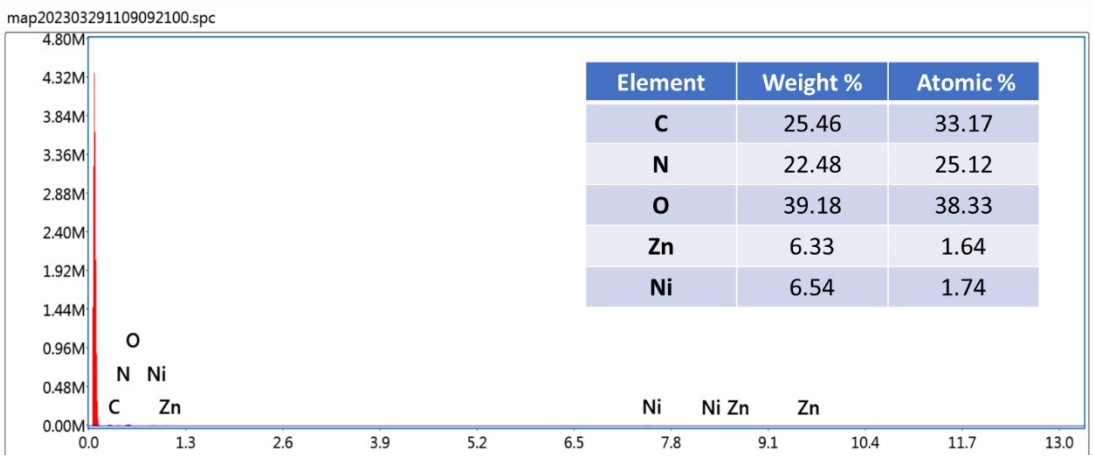

Element	Weight %	Atomic %
C	25.46	33.17
N	22.48	25.12
O	39.18	38.33
Zn	6.33	1.64
Ni	6.54	1.74

Fig. S4: EDX analysis of $Ni(OH)_2$/ZNC@rGO catalyst.

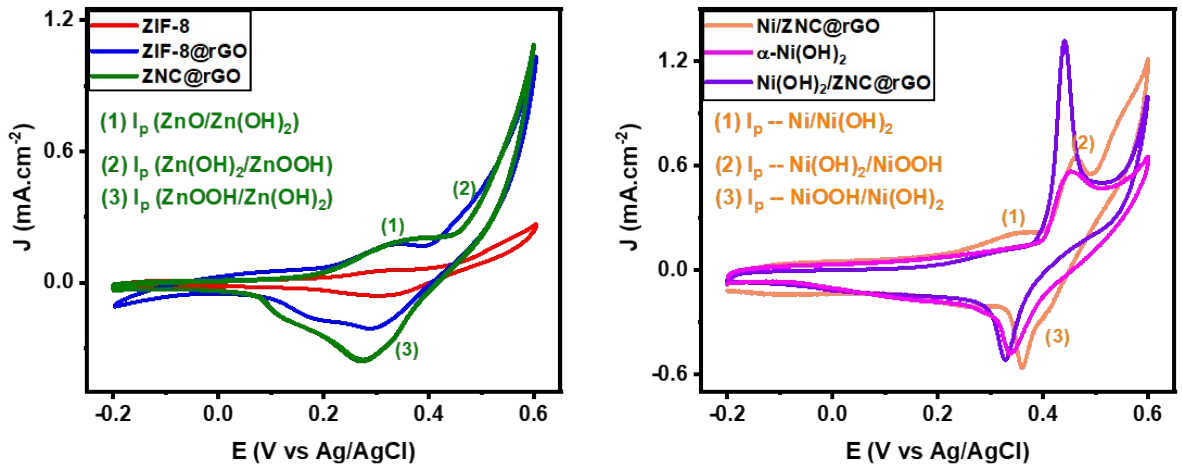

Fig. S5: CV curves of (a) ZIF-8, ZIF-8@rGO, and ZNC@rGO and (b) Ni/ZNC@rGO, α-$Ni(OH)_2$, and $Ni(OH)_2$/ZNC@rGO recorded at 50 mV s^{-1} in 1M KOH.

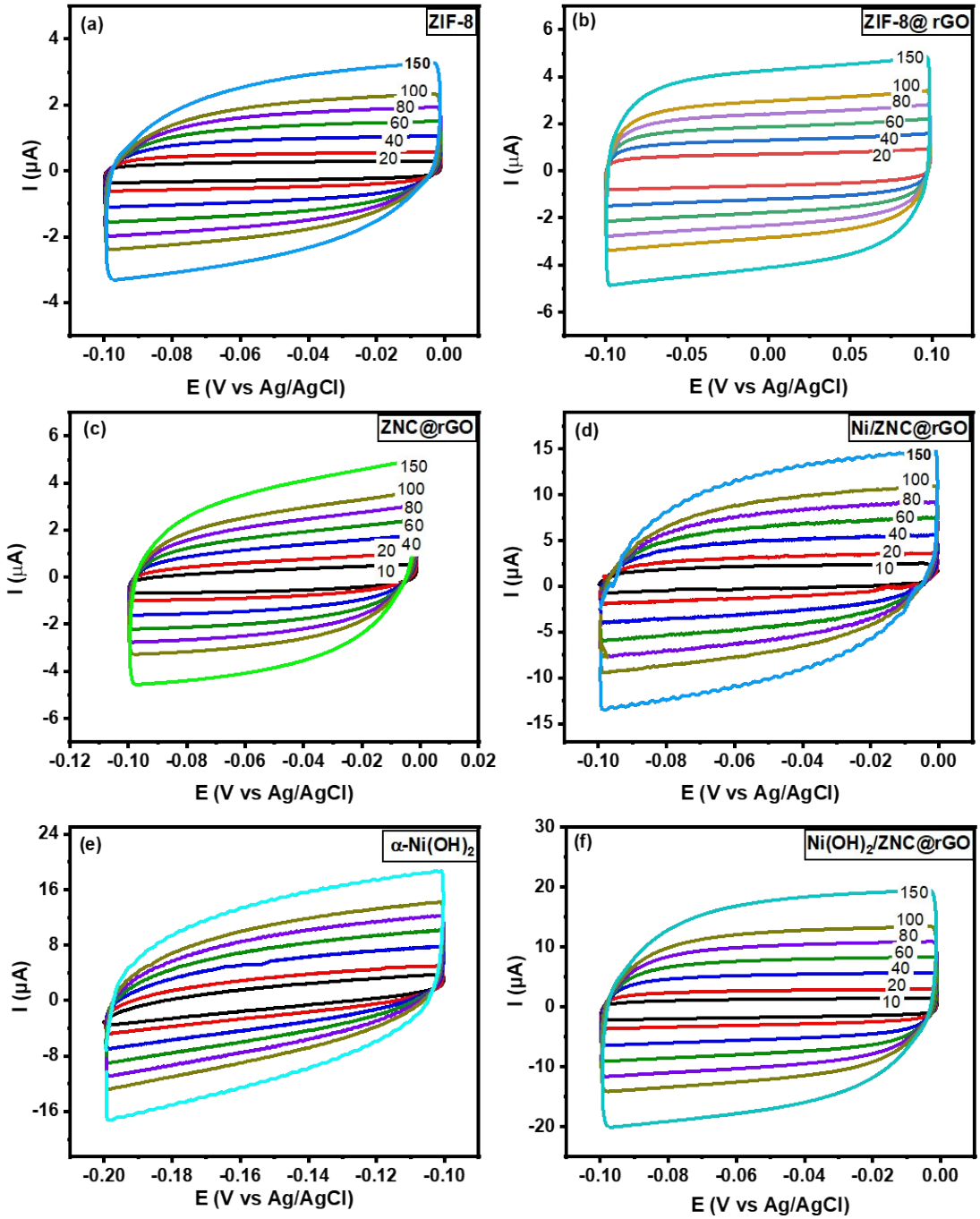

Fig. S6: CV curves recorded in 1M KOH in the potential range of 0- 0.1 V at different scan rates for (a) ZIF-8, (b) ZIF-8@rGO, (c) ZNC@rGO, (d) Ni/ ZNC@rGO, (e) αNi(OH)$_2$, and (f) Ni(OH)$_2$/ ZNC@rGO.

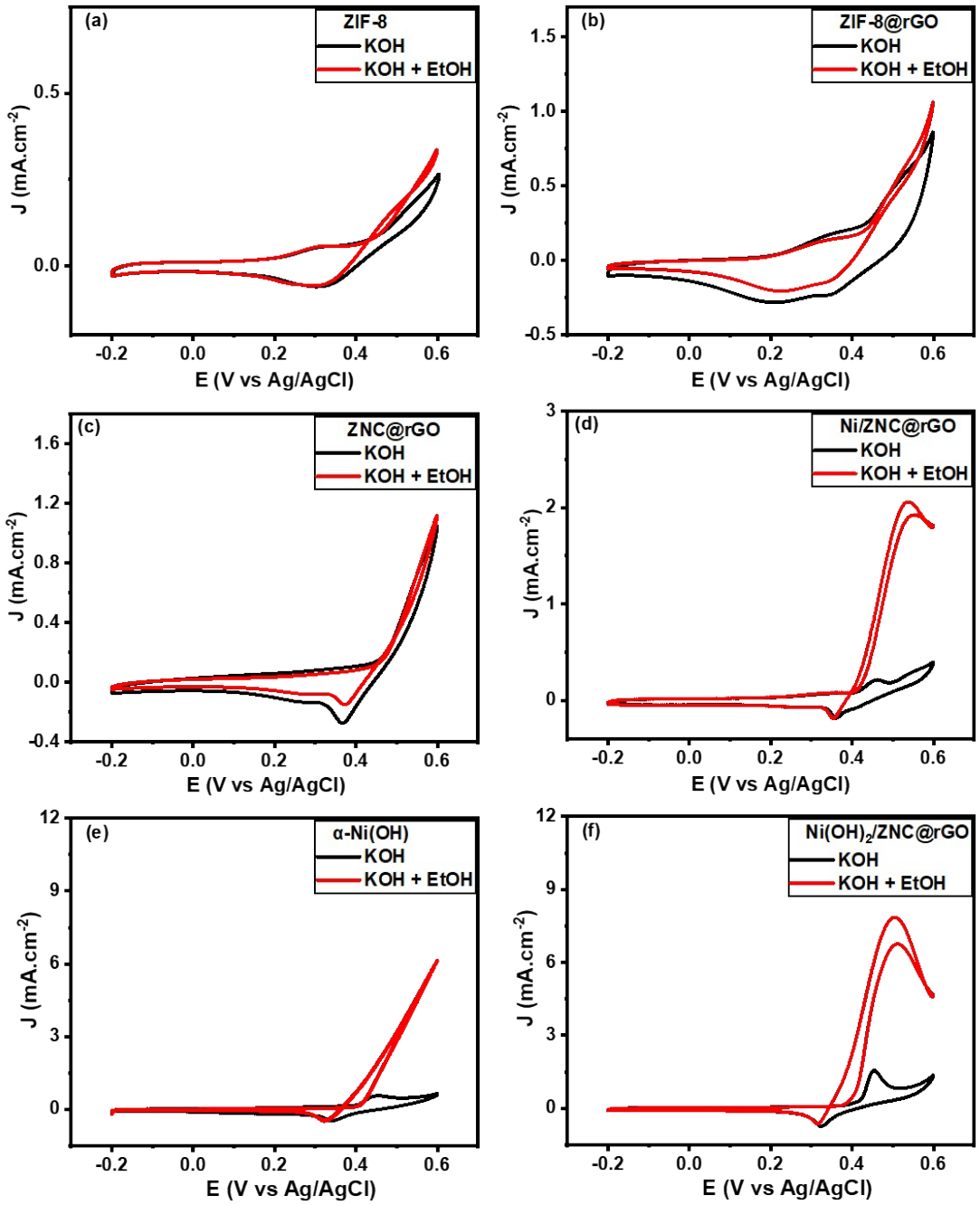

Fig. S7: CV curves of (a) ZIF-8, (b) ZIF-8@rGO, (c) ZNC@rGO, (d) Ni/ ZNC@rGO, (e) α-$Ni(OH)_2$ and (f) $Ni(OH)_2$/ ZNC@rGO in the absence and presence of 1M ethanol at a scan rate of 50 mV s^{-1}.

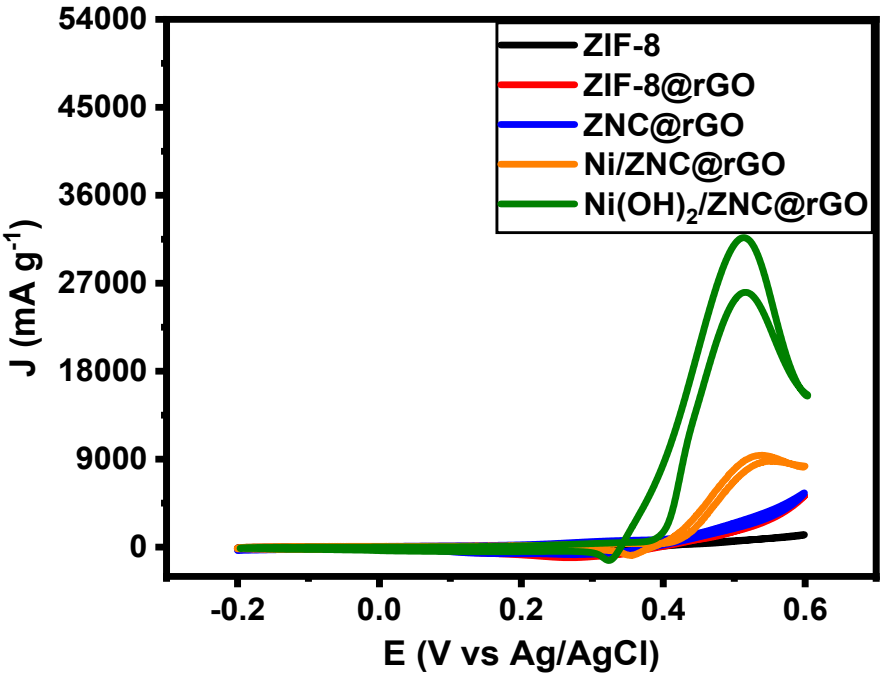

Fig. S8: CV curve of the as-prepared catalysts in 1M KOH + 1M Ethanol at a scan rate of 50 mV s^{-1}.

Table 1: Comparison of the prepared catalyst for EOR efficiency with some modified electrodes vs Ag/AgCl.

Working electrode	**C_{EtOH} (M)**	**E_{onset} (V)**	**E_{pa} (V)**	**I_{pa} (mA/cm^2)**	**Ref.**
NiCo/ErN-GO/CCE	0.1	0.38	0.81	64.23	[1]
Ni(II)(Phen)$_2$/rGO-modified PGE	1.0	0.4	0.53	0.81	
NiPPy/GCE	0.9	---	0.55	8.50	[2]
Ni/p(NMA)/MCPE	0.4	0.46	0.66	1.80	[3]
CPE@[Ni(cis-salcn)]	0.5	0.42	0.55	2.60	[4]
CM-ZnO	2.0	0.40	0.58	35.0	[5]
Cu_2O/PPy/CPE	0.2	0.58	0.80	2.25	[6]
4-trifluoromethylphenyl (TFMP)-Pt/C	1.0	-0.489	-----	776	[7]
NiO@PPC-600	1.0	1.1 (vs RHE)	1.4 (vs RHE)	231.8	[8]
Ni,Fe_2O_3/Cu Cu/Ni,Fe_2O_3	1.0	0.31 0.31	0.476 0.510	0.492 0.644	[9]
Microbead-encapsulated ZnO particles derived from coffee waste	2.0	0.4	0.5	35	[5]
Ag/Ag_2O	1.5	0.43	0.5	69	[10]
Ni(OH)$_2$/ ZNC@rGO	**1.0**	**0.34**	**0.51**	**8.30**	**This work**

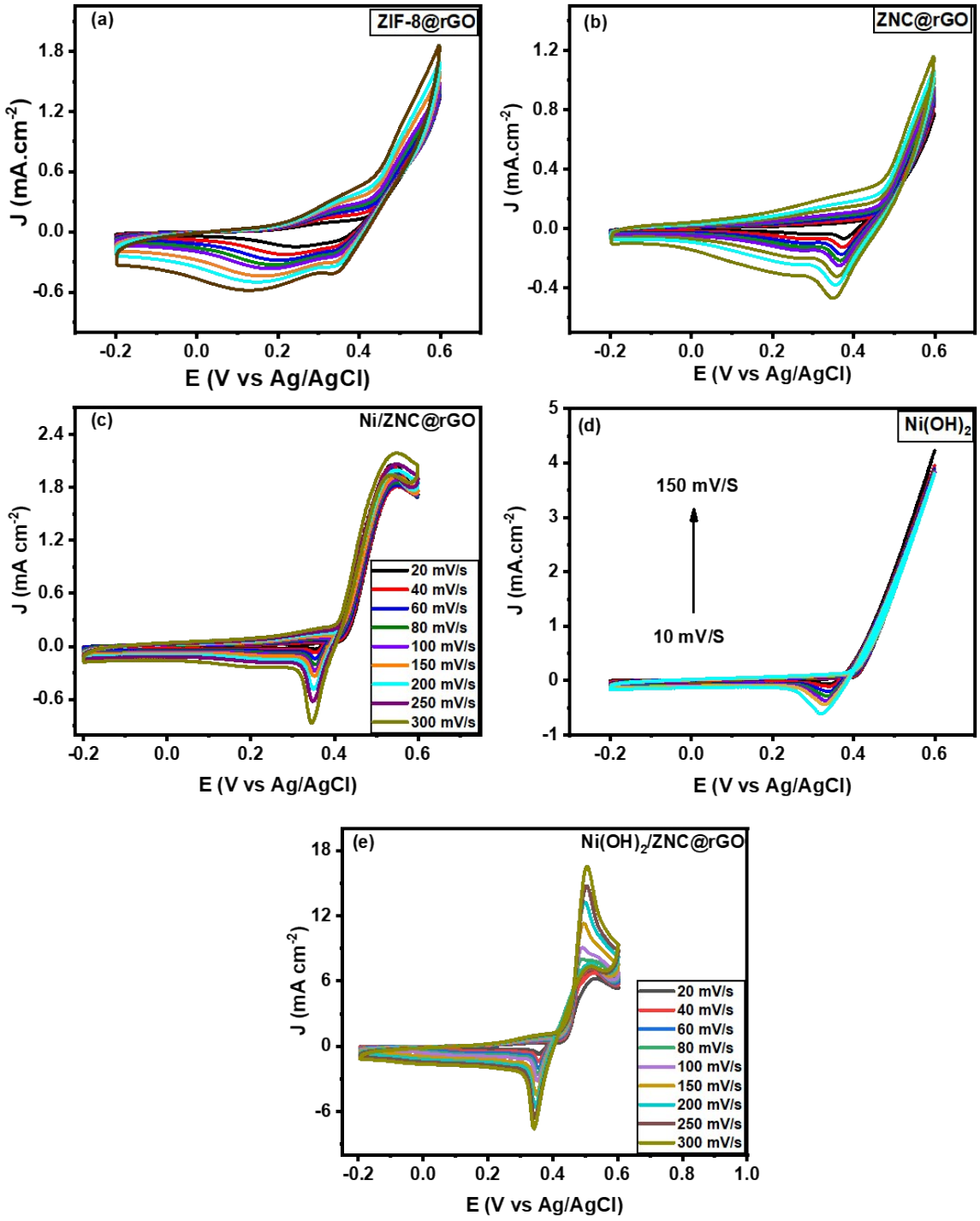

Fig. S9: CV curves recorded in 1M KOH in the potential range of -0.2- 0.6 V at different scan rates for (a) ZIF-8@rGO, (b) ZNC@rGO, (c) Ni/ ZNC@rGO, (d) α-$Ni(OH)_2$, and (e) $Ni(OH)_2$/ ZNC@rGO catalysts.

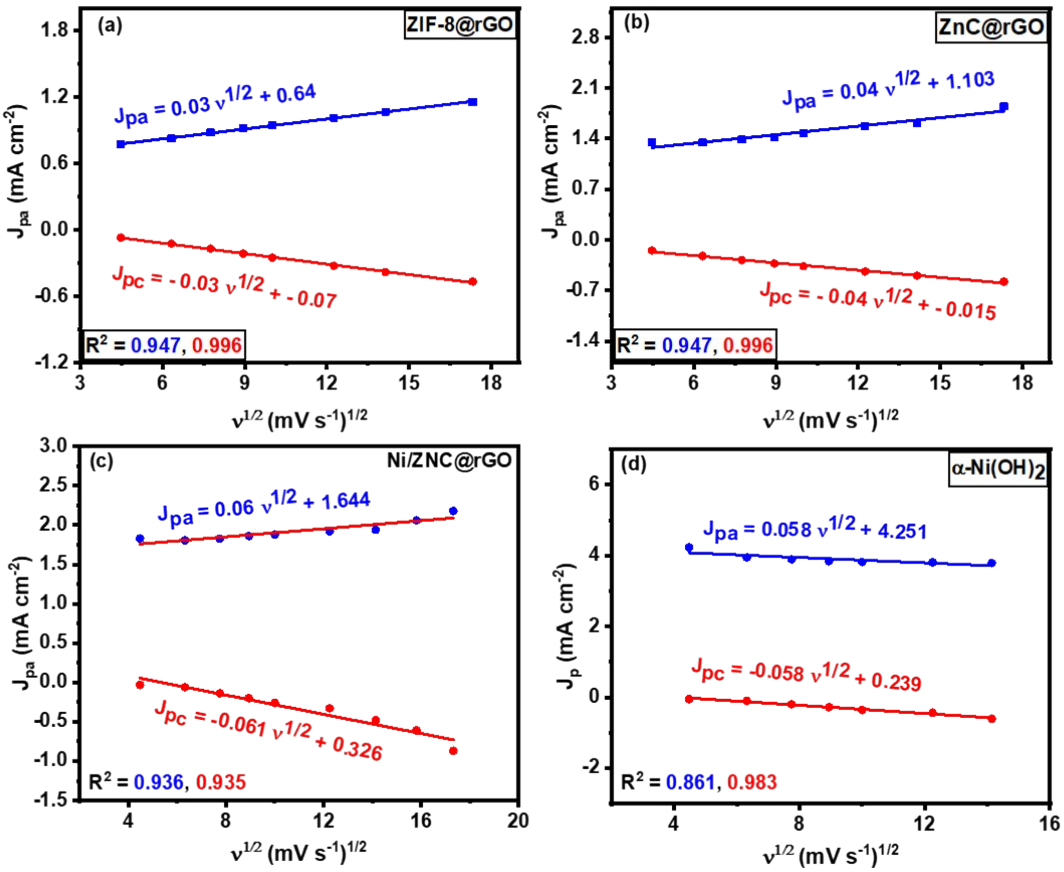

Fig. S10: Linear relationship of anodic (I_{pa}) and cathodic current (I_{pc}) densities of (a) ZIF-8@rGO, (b) ZNC@rGO, (c) Ni/ZNC@rGO, and (d) α-$Ni(OH)_2$ versus the square root of scan rates.

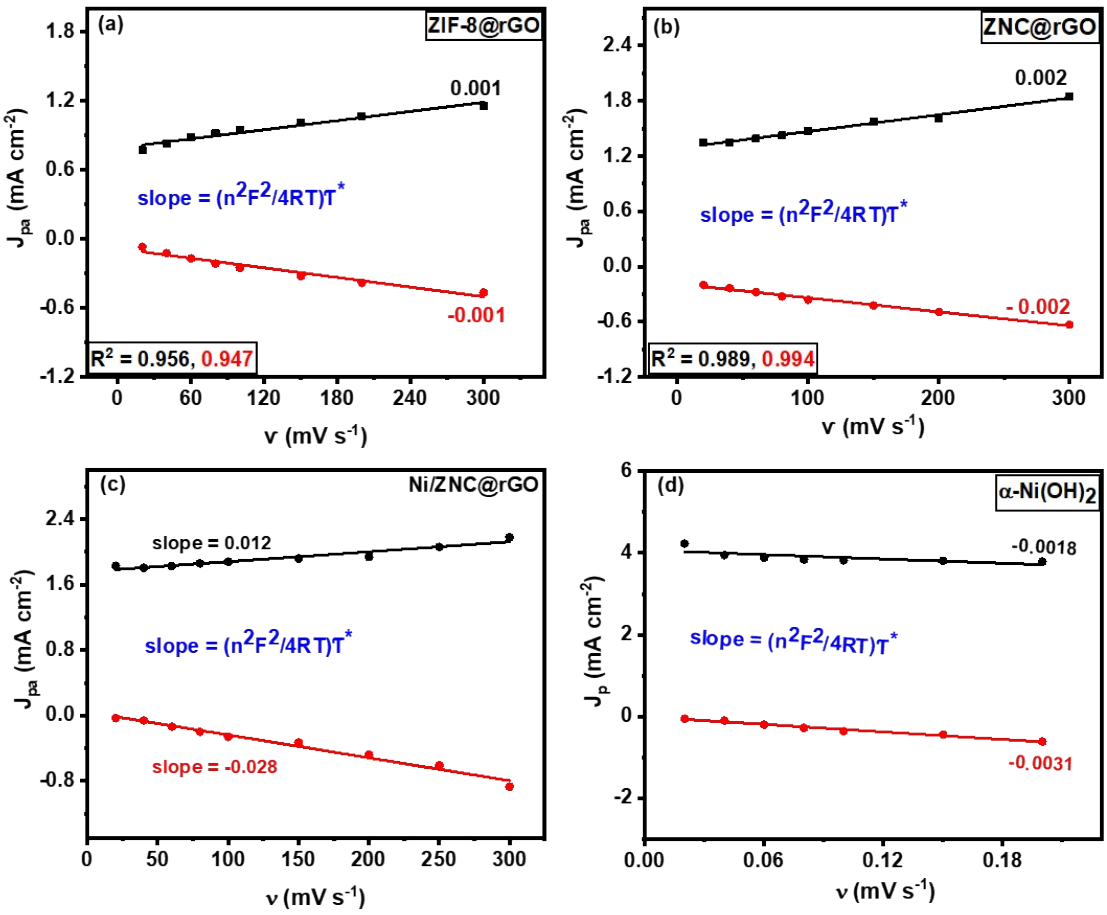

Fig. S11: Linear relationship of anodic (I_{pa}) and cathodic current (I_{pc}) densities of (a) ZIF-8@rGO, (b) ZNC@rGO, (c) Ni/ZNC@rGO, and (d) α-$Ni(OH)_2$ versus the scan rates.

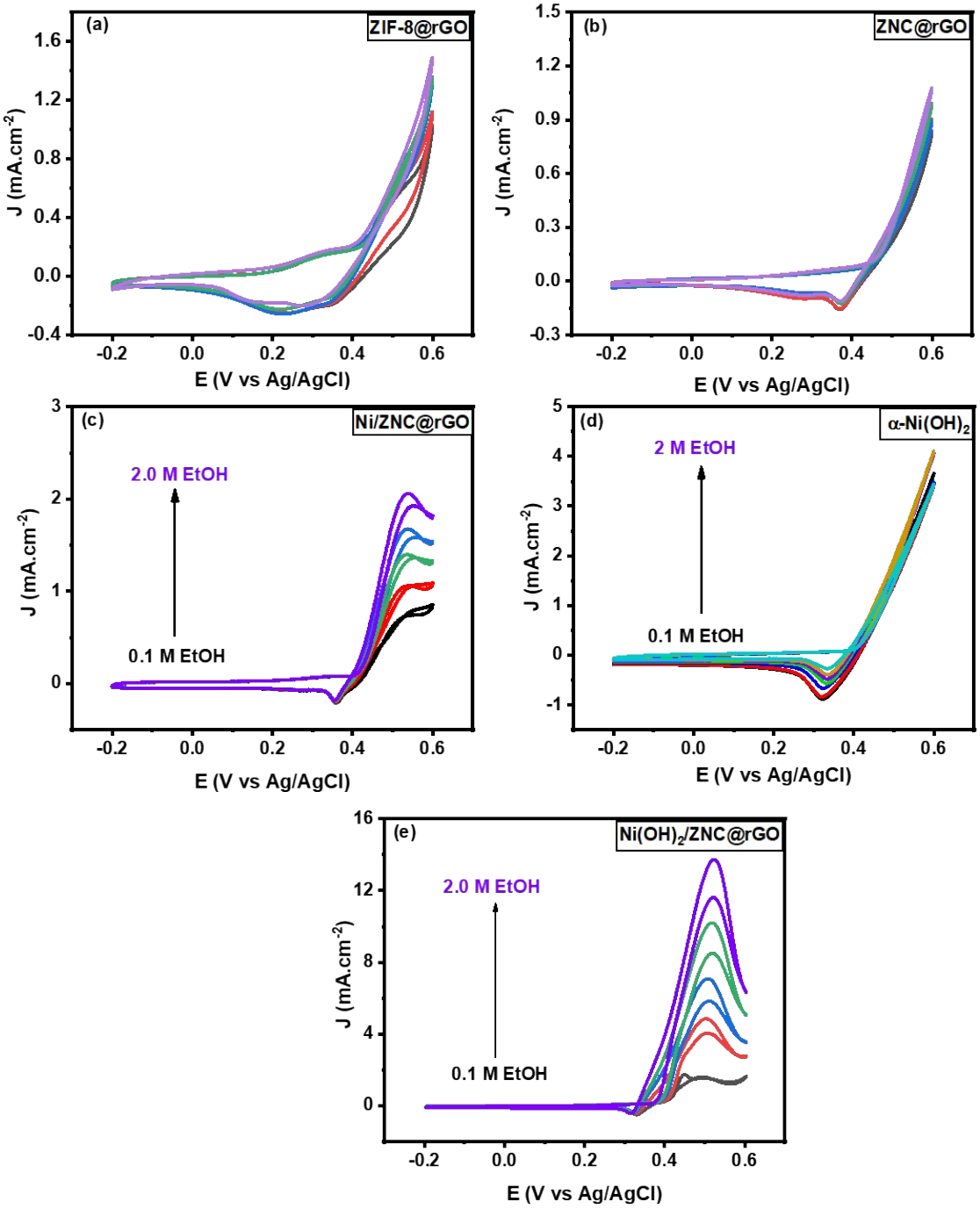

Fig. S12: CV of (a) ZIF-8@rGO, (b) ZNC@rGO, Ni/ ZNC@rGO, (d) α-$Ni(OH)_2$ and (e) $Ni(OH)_2$/ ZNC@rGO catalysts in 1M KOH with different concentrations of ethanol (0.1- 2.0 M).

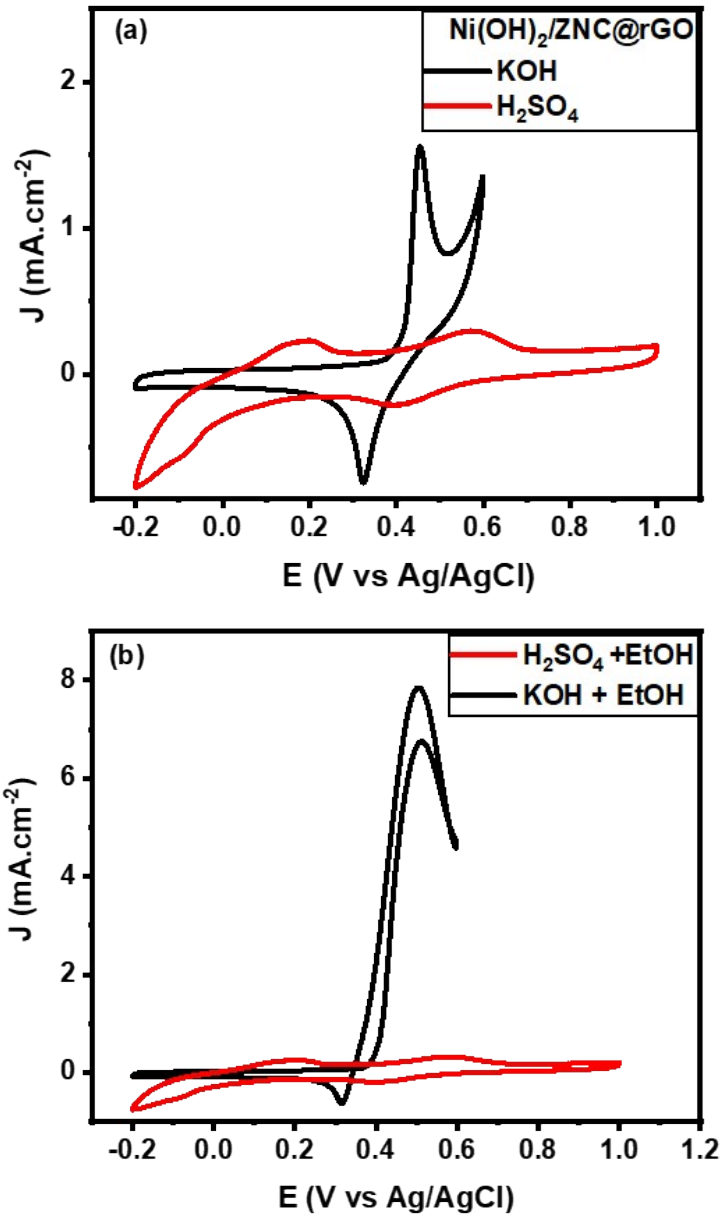

Fig. S13: CV of $Ni(OH)_2$/ ZNC@rGO in (a) 1M of alkaline and acidic electrolyte and (b) 1M of EtOH+ 1M of alkaline or acidic medium.

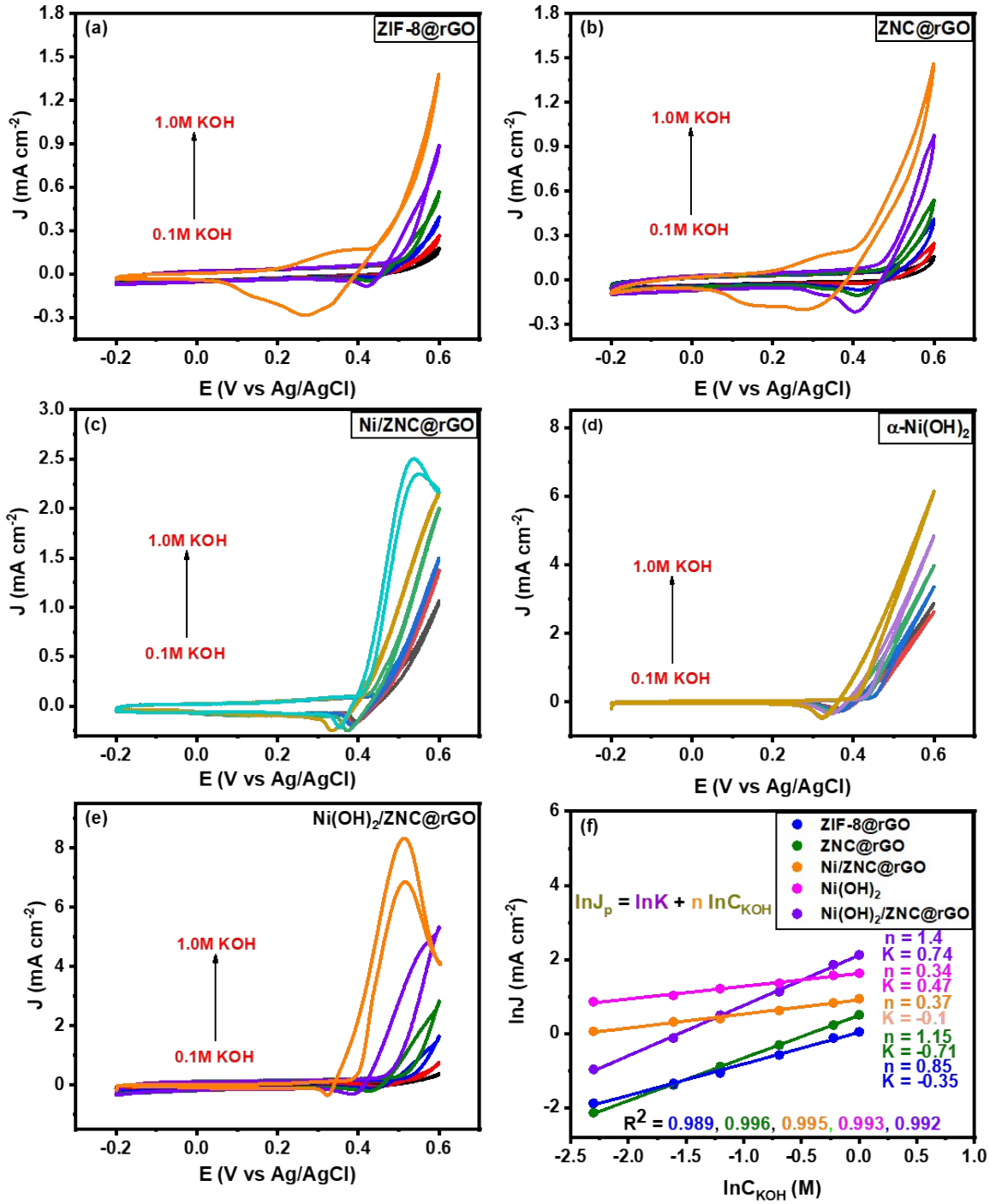

Fig. S14: CV of (a) ZIF-8@rGO, (b) ZNC@rGO, (c) Ni/ ZNC@rGO, (d) α-$Ni(OH)_2$ and (e) $Ni(OH)_2$/ ZNC@rGO catalysts in 1M EtOH with different concentrations of KOH electrolyte (0.1- 1.0 M) and (f) effect of concentration of the KOH electrolyte in electrocatalytic ethanol oxidation.

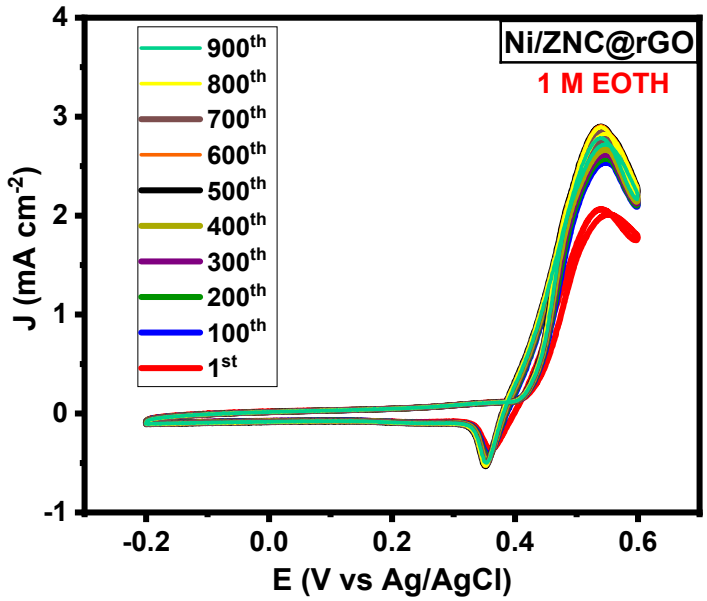

Fig. S15: CVs curves for 900 cycles from -0.2- 0.6 V at a scan rate of 10 mV s^{-1} in 1M KOH+ 1M EtOH using Ni/ ZNC@rGO.

References

1. K. Rahmani and B. Habibi, *RSC Adv*, 2019, **9**, 34050-34064.
2. A. Ehsani, M. G. Mahjani, M. Jafarian and A. Naeemy, *Electrochim Acta*, 2012, **71**, 128-133.
3. J.-B. Raoof, A. Omrani, R. Ojani and F. Monfared, *Journal of Macromolecular Science, Part A*, 2013.546-541 ,50 ,
4. G. V. Lima, L. dos Santos Mello, E. R. Dockal and M. Firmino de Oliveira, *Microchemical Journal*, 2022, **175**, 107209.
5. Z. K. Ghouri, K. Elsaid, A. Abdel-Wahab, A. Abdala and M. Z. Farhad, *J Mater Sci: Mater Electron*, 2020, **31**, 6530-6537.
6. A. El Attar, L. Oularbi, S. Chemchoub and M. El Rhazi, *Int J Hydrogen Energy*, 2020, **45**, 8887-8898.
7. C. Han, Y. Lyu, S. Wang, B. Liu, Y. Zhang, J. Lu and H. Du, *Carbon Energy*, 2023, **5**.
8. N. Gao, L. Gao, X. Zhang, Y. Zhang and T. Hu, *J Alloys Compd*, 20.169485 ,947 ,23
9. M. Ghalkhani, R. Abdullah Mirzaie, A. Banimostafa, E. Sohouli and E. Hashemi, *Int J Hydrogen Energy*, 2023, **48**, 21214-21223.
10. M. G. A. Saleh, S. A. El Wanees, I. D. Alruwaili, A. Akremi, A. M. Elbasiony and M. Brakat, *Int. J. Electrochem. Sci.*, 2023, **18**, 100372.